Modified magnetic anisotropy at $LaCoO_3/La_{0.7}Sr_{0.3}MnO_3$ interfaces

M. Cabero, K. Nagy, F. Gallego, A. Sander, M. Rio, F. A. Cuellar, J. Tornos, D. Hernandez-Martin, N. M. Nemes, F. Mompean, M. Garcia-Hernandez, A. Rivera-Calzada, Z. Sefrioui, N. Reyren, T. Feher, M. Varela, C. Leon, and J. Santamaria

Citation: APL Materials **5**, 096104 (2017);

View online: https://doi.org/10.1063/1.5002090

View Table of Contents: http://aip.scitation.org/toc/apm/5/9

Published by the American Institute of Physics

APL MATERIALS **5**, 096104 (2017)

Modified magnetic anisotropy at $LaCoO_3/La_{0.7}Sr_{0.3}MnO_3$ interfaces

M. Cabero,[1,2,3,4] K. Nagy,[5] F. Gallego,[1,2] A. Sander,[6] M. Rio,[1,2] F. A. Cuellar,[1,2] J. Tornos,[1,2] D. Hernandez-Martin,[1,2] N. M. Nemes,[1,2] F. Mompean,[2,7] M. Garcia-Hernandez,[2,7] A. Rivera-Calzada,[1,2] Z. Sefrioui,[1,2,4] N. Reyren,[6] T. Feher,[5] M. Varela,[1,3,4] C. Leon,[1,2,4] and J. Santamaria,[1,2,4,a]

[1]*GFMC, Departamento de Fisica de Materiales, Universidad Complutense de Madrid, 28040 Madrid, Spain*
[2]*Unidad Asociada ICMM-CSIC "Laboratorio de Heteroestructuras con Aplicacion en Espintronica," UCM, CSIC, 28049 Madrid, Spain*
[3]*Instituto Pluridisciplinar, Universidad Complutense de Madrid, 28040 Madrid, Spain*
[4]*Instituto de Magnetismo Aplicado, Universidad Complutense de Madrid, 28040 Madrid, Spain*
[5]*Department of Physics, Budapest University of Technology and Economics, MTA-BME Lendület Magneto-Optical Research Group, MTA-BME Condensed Matter Physics Research Group, 1111 Budapest, Hungary*
[6]*Unité Mixte de Physique, CNRS, Thales, Univ. Paris-Sud, Université Paris-Saclay, 91767 Palaiseau, France*
[7]*Instituto de Ciencia de Materiales de Madrid ICMM-CSIC, Calle Sor Juana Inés de la Cruz, 3, 28049 Madrid, Spain*

(Received 29 March 2017; accepted 29 August 2017; published online 15 September 2017)

Controlling magnetic anisotropy is an important objective towards engineering novel magnetic device concepts in oxide electronics. In thin film manganites, magnetic anisotropy is weak and it is primarily determined by the substrate, through induced structural distortions resulting from epitaxial mismatch strain. On the other hand, in cobaltites, with a stronger spin orbit interaction, magnetic anisotropy is typically much stronger. In this paper, we show that interfacing $La_{0.7}Sr_{0.3}MnO_3$ (LSMO) with an ultrathin $LaCoO_3$ (LCO) layer drastically modifies the magnetic anisotropy of the manganite, making it independent of the substrate and closer to the magnetic isotropy characterizing its rhombohedral structure. Ferromagnetic resonance measurements evidence a tendency of manganite magnetic moments to point out-of-plane suggesting non collinear magnetic interactions at the interface. These results may be of interest for the design of oxide interfaces with tailored magnetic structures for new oxide devices. [http://dx.doi.org/10.1063/1.5002090]

Interfaces between correlated oxides are focusing great interest due to the emergent electronic states which result from the different forms of electronic, spin, and lattice reconstructions.[1,2] Many of these oxides share a common perovskite structure with similar lattice parameters, enabling highly perfect interfaces in epitaxial heterostructures. Strain has often been employed as a powerful handle to control their nucleation due to its effect on the orbital polarization.[3] Recently, it has been found that strain induced structural distortions offer an additional, subtler knob to control degrees of freedom such as magnetism that are often not accessible to other external perturbations.[4] Different degrees of rotations of the oxygen octahedra around the individual axes are driven by the difference between ionic radii and by the different structural instabilities dictated by symmetry.[5–7] These rotations have a direct effect on the crystal field experienced by the electronic *d* manifold of the B site atom and

[a]Present address: Unité Mixte de Physique, CNRS, Thales, Univ. Paris-Sud, Université Paris-Saclay, 91767 Palaiseau, France.

are at the root of different forms of orbital ordering that change the energy hierarchy of crystal field levels.[5] Octahedral rotations can be transmitted across an interface by choosing a substrate or a buffer layer with the desired pattern of rotations; this has enabled deep changes in the magnetic anisotropy of manganites[5] or ruthenates.[6,7]

In this paper, we have interfaced $La_{0.7}Sr_{0.3}MnO_3$ (LSMO) with an ultrathin layer of $LaCoO_3$ (LCO). Structurally, LCO is an interesting system because it possesses the same rhombohedral R-3c space group as LSMO, with the same $a^-a^-a^-$ pattern of octahedral rotations[8,9] that may ideally enable interesting forms of coupling between the magnetic orders of both materials.[10] We will show how structural distortions, possibly resulting from arrays of oxygen vacancies in LCO, can propagate through the coherent epitaxial interface and have drastic effects on the magnetic anisotropy of the manganite layer grown on top. The control of magnetic anisotropy is of the utmost importance for practical applications in magnetic recording or other magnetic sensor devices because it dictates the mechanism of magnetization reversal (rotation vs. domain nucleation) when changing the magnetic field.

Among the different oxides, LSMO has been widely studied as a magnetic electrode in (laboratory scale) magnetic devices and sensors for its high degree of spin polarization and its Curie temperature (T_C = 350 K) above room temperature.[11,12] The strong electron lattice coupling of manganites is responsible for the almost complete quenching of the orbital moment. The spin orbit interaction acts thus through higher order processes and, as a result, magnetic anisotropy is weak.[13] In cobaltites, the spin orbit interaction is much stronger due to the unquenched orbital moment acting on degenerate t_{2g} crystal field levels.[13] The crystal field experienced by the d states of the trivalent Co ion has an energy scale comparable to the Hund coupling interaction.[14,15] As a result, $LaCoO_3$ (LCO) bulk samples can experience a spin state transition between the low spin (LS), S = 0 with full t_{2g} manifold, the intermediate spin (IS) with spin S = 1 where one electron is promoted to the e_g state, and the high spin (HS) S = 2 with four unpaired electrons, two in e_g and two in t_{2g} levels. The transition from the non magnetic state into the paramagnetic state experienced by bulk LCO samples below 90 K is attributed to the transition from the LS into IS or HS.[14–19] In tensile strained thin films, this transition occurs into a ferromagnetic insulating state,[20–27] which is driven by the spin state probably concomitant with orbital order.[28]

Samples for this study were grown epitaxially on $SrTiO_3$ (STO) (001) substrates by a high pressure pure oxygen (3.2 mbar) ac sputtering apparatus at elevated temperatures (750 °C for LCO and 900 °C for LSMO), which produced good epitaxial properties.[29] SQUID magnetometry evidenced that the single cobaltite layers grown epitaxially on STO substrates were insulating and ferromagnetic below 80 K as previously found by others. The LSMO single films (18 nm thick) were ferromagnetic and metallic up to 350 K. Matching to the in-plane cubic structure of STO suppresses the octahedral rotations characteristic of the rhombohedral symmetry and a cubic undistorted manganite structure results over a thickness range of several nanometers.[30] Two kinds of bilayer samples with the same thickness of LSMO (18 nm) and LCO (3 nm) were prepared with different layer sequences, namely, $LSMO_{18nm}/LCO_{3nm}$ with a cobaltite top layer (//LSMO/LCO) and $LCO_{3nm}/LSMO_{18nm}$ where the manganite was grown on a cobaltite buffer layer (//LCO/LSMO).

Both kinds of bilayers were epitaxial and of good structural quality. Epitaxial growth is shown by high angle x-ray diffraction (XRD) θ-2θ scans in Fig. 1(a). Also, the presence of finite size oscillations in the low angle x-ray reflectivity (XRR) denotes that layers are flat and continuous over lateral distances of the order of the structural coherence length (around a micron for XRR). Figure 1(b) exhibits rocking curves around the (002) peak of the manganite layer in both bilayer samples, which show identical half maximum widths of 0.03°. However, rocking curves from the //LCO/LSMO sample (red data) display wider peak tails which we attribute to non-specular scattering arising from local perturbations of the crystalline order. Reciprocal space maps [Fig. 1(c)] were acquired around the asymmetric (−1 0 3) reflection of the manganite using a PANalytical Empyrean diffractometer equipped with a Cu source and a PIXcel3D detector. It can be observed that the manganite layers are uniformly strained to match the cubic in-plane lattice parameters of STO, which imposes a tensile epitaxial mismatch strain amounting 0.5% for LSMO (a = 3.87 Å) and 2% for LCO (a = 3.82 Å). The slightly larger c lattice parameter of the manganite in the //LCO/LSMO sample (3.843 Å) as compared with 3.835 Å found for the //LSMO/LCO sample indicates that the LCO buffer layer has a structural effect beyond contributing to lattice strain relaxation, which would modify the

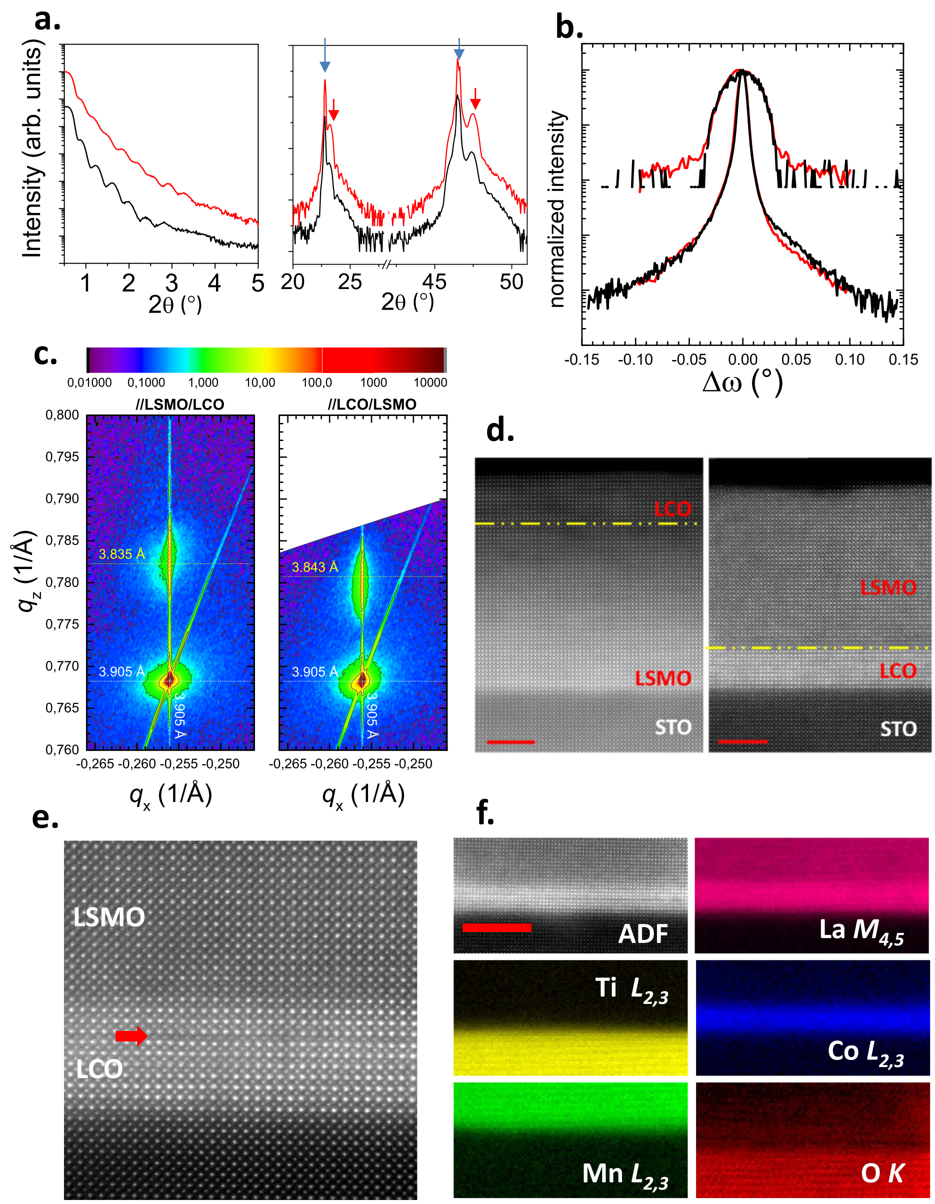

FIG. 1. (a) XRR (left) and XRD (right) patterns of two bilayers with different sequences. The red curve corresponds to the STO(100)//LCO_{3nm}/$LSMO_{18nm}$ (//LCO/LSMO) bilayer, while the black curve represents the STO(100)//$LSMO_{18nm}$/LCO_{3nm} (//LSMO/LCO) specimen. Blue arrows in XRD patterns indicate the STO(001) substrate reflections, while red arrows indicate the LSMO/LCO peak. (b) Rocking curves around the (002) manganite for //LCO/LSMO (red) and //LSMO/LCO (black). As a reference, rocking curves of substrate STO peaks have been also included. (c) Reciprocal space maps around the (−103) reflection for //LCO/LSMO (right plot) and //LSMO/LCO (left plot). (d) Atomic resolution high angle annular dark field (HAADF) images of a //LSMO/LCO (left) and a //LCO/LSMO (right) bilayer. The yellow dashed lines indicate the interfaces between the LSMO and LCO layers, which have been placed at 50% of the STEM image contrast change observed between both materials. The scale bars represent 5 nm. (e) High resolution HAADF image of a //LCO/LSMO bilayer. The red arrow indicates a dark stripe within the LCO layer which would result from the presence of O-deficient CoO_{2-x} atomic planes. (f) EELS chemical maps extracted from the Ti $L_{2,3}$ (yellow), O K (red), Mn $L_{2,3}$ (green), Co $L_{2,3}$ (blue), and La $M_{4,5}$ (pink), edges of an atomic resolution 2D EEL-spectrum image, along with the simultaneously acquired HAADF signal. Some spatial drift in the sample was present during acquisition. The scale bar is 8 nm.

in-plane lattice parameters (not observed). The interfaces are coherent, as evidenced by images of aberration corrected scanning transmission electron microscopy (STEM) combined with electron energy-loss spectroscopy (EELS) acquired at 200 kV in JEOL ARM200cF equipped with a spherical aberration corrector and a Gatan Quantum spectrometer [see Figs. 1(d)–1(f)]. Atomic resolution STEM images of cross section samples prepared down the pseudocubic [100] direction show that, independent of the layer sequence, no extended defects such as mismatch dislocations are observed. High resolution STEM images display local undulations of the (001) planes of the cobaltite, along with changes in the contrast of the annular dark field STEM images, where dark Co–O planes are observed within the LCO layers. In fact, these dark stripes would be O-deficient CoO_{2-x} atomic planes [see Fig. 1(e)], which usually result from the presence of arrays of oxygen vacancies in LCO[26,27] and also in Sr-doped cobaltites. In fact, measurements of the out-of-plane lattice parameter of LCO showed values of 3.89 Å, larger than expected, probably due to the presence of oxygen vacancies. Such arrays constitute an efficient mechanism to release epitaxial strain in cobaltite thin films.[31] An upper estimate to the width of the LCO/LSMO interfaces was obtained from quantifying the width of the 25%-75% jump of the different chemical profiles obtained from EELS images. Values obtained lie in the 0.7-1 nm range, around two perovskite blocks, showing that any chemical or physical disorder (interdiffusion or step disorder) is highly confined, i.e., the interfaces are relatively sharp.

$M(H)$ loops performed on both kinds of bilayers with magnetic fields aligned with relevant [100], [110] (in-plane), and [001] (out-of-plane) directions show profound changes in magnetic response (see Fig. 2). //LSMO/LCO samples display a biaxial in-plane anisotropy with biaxial easy axes as shown previously in single layer manganites.[30,32–35] At high magnetic fields (~2 T), magnetization saturates to the same value in the three different directions. A substantial remanence is observed in out-of-plane loops, as previously found in single manganite thin films.[36] The magnetization lies in-plane, as expected for a moderate out-of-plane anisotropy K_{2c} (crystalline or interfacial), smaller than the shape anisotropy $\mu_0 M_s^2/2 \approx 200$ kJ/m^3 ($M_s \approx 560$ kA/m). In fact, calculating the effective out-of-plane anisotropy K_{eff} by considering the saturation field yields values of $K_{\mathrm{eff}} \approx \mu_0 H_K M_s \approx 220$ kJ/m^3, which indicates K_{2c} smaller than a few tens of kJ/m^3. On the other hand, //LCO/LSMO samples were magnetically very different. $M(H)$ loops indicate a negligible in-plane anisotropy and very small effective out-of-plane anisotropy, indicating on the contrary a much larger out-of-plane anisotropy partially compensating the shape anisotropy. Compared to //LSMO/LCO, //LCO/LSMO hence displays a stronger out-of-plane structural (crystalline or interfacial) anisotropy, but weaker in-plane anisotropies, resembling the magnetic structure of the rhombohedral structure of bulk LSMO samples.[37]

To get further insight into the changes in the magnetic anisotropy induced by the ultrathin cobaltite buffer layer, we have conducted ferromagnetic resonance (FMR) experiments on both bilayers //LSMO/LCO and //LCO/LSMO, with cobaltite top and bottom layers. The FMR was measured at 77 K and 9 GHz, being the magnetic field swept along various directions. The angular dependence of the FMR for the two samples studied is shown in Fig. 3. For rotations in the (010) plane, we define the orientation as θ, where θ = 0° refers to B//[001] and θ = 90° to B//[100] configurations, while

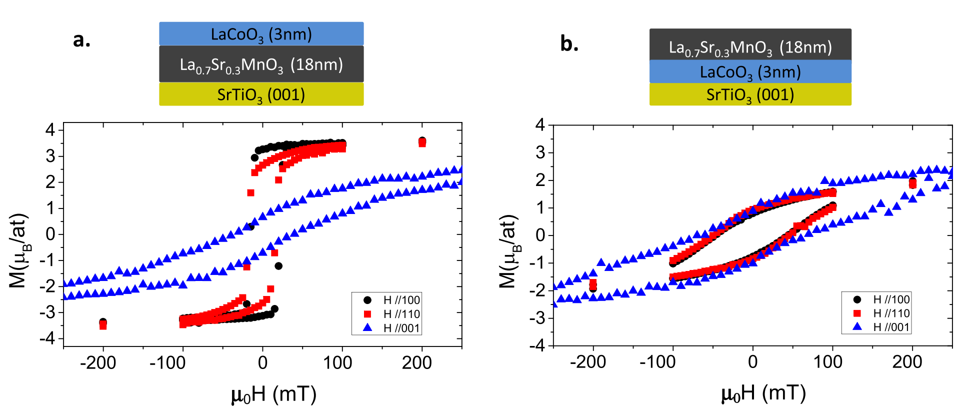

FIG. 2. M(H) loops of //LSMO/LCO (a) and //LCO/LSMO (b) at 5 K with magnetic fields applied in-plane along [100] (black circles) and [110] (red squares) in-plane directions and in the [001] direction out-of-plane (blue triangles).

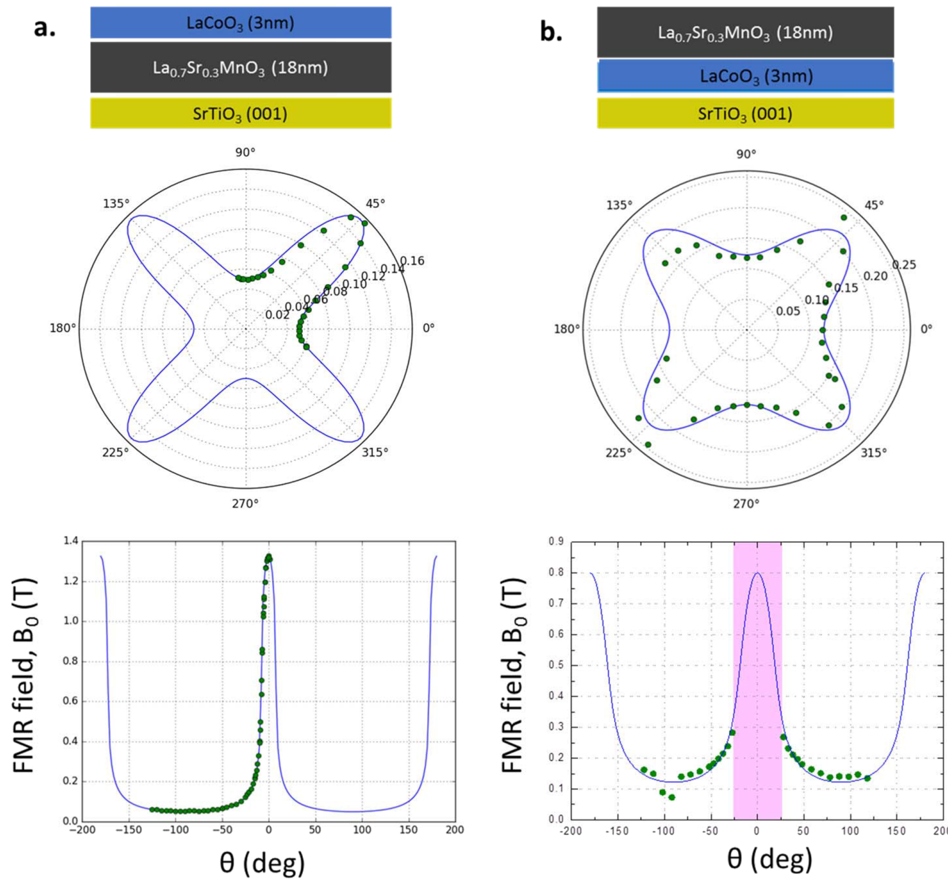

FIG. 3. Ferromagnetic resonance fields at 9.4 GHz and 77 K in (a) the //LSMO/LCO and (b) the //LCO/LSMO bilayer samples. The polar plots show orientation dependence for magnetic field rotated in the (001) plane, and the plots below show out-of-plane rotations. Symbols show actual measurements, while continuous lines are simulations based on Eq. (1) with parameters defined in the main text. FMR was much broader in the //LCO/LSMO sample and the pink band in the out-of-plane rotation marks the region where FMR broadened to a level that rendered the FMR field evaluation unreliable.

for rotations in the (001) plane, we define the orientation with ϕ, where $\phi = 0°$ refers to a B//[100] orientation while $\phi = 45°$ corresponds to a B//[110] configuration. The four minima of the FMR field, the radial value of the polar plot, along the [100] directions indicate the magnetic easy axes. These data can be explained in terms of the anisotropic magnetic free energy density,

$$f = -\mu_0 \boldsymbol{M} \cdot \boldsymbol{B_0} + (\frac{1}{2}\mu_0 {M_S}^2 + K_{2c})\alpha_3^2 + K_{4ab}\left(\alpha_1^4 + \alpha_2^4\right) + K_{4c}\alpha_3^4, \quad (1)$$

which contains the Zeeman, demagnetizing, and magnetic anisotropy terms. In this expression, M_S is the saturation magnetization of the LSMO ferromagnetic layer, α_1, α_2, and α_3 are the direction cosines of the LSMO magnetization ($\alpha_i = M_i/M_S$, i = 1,2,3, and $\alpha_1^2 + \alpha_2^2 + \alpha_3^2 = 1$), K_{2c} is the lowest order in-plane anisotropy term, and K_{4ab} and K_{4c} account for a higher order in-plane and out-of-plane crystalline anisotropy, respectively.[38] The shape anisotropy due to the planar geometry of the thin layers adds a term indistinguishable from the K_{2c} term without extra input. We define the magnitude of this shape anisotropy by setting $\mu_0 M_S = 0.75$ T, which is equivalent to an extra easy-plane anisotropy with $K_{2c} = 220$ kJ/m^3.

For both bilayers //LSMO/LCO and //LCO/LSMO, we obtained $K_{4ab} = -8.3$ kJ/m^3 and $K_{4c} = 0$ since no higher order terms were needed for the description of the important features. However, while for //LSMO/LCO, $K_{2c} = 71$ kJ/m^3, for the //LCO/LSMO bilayer, the negative value of $K_{2c} = -83$ kJ/m^3 indicates that without the shape anisotropy the magnetization would be perpendicular to the (001) plane. At room temperature, the anisotropies drop by about one order of magnitude, but [100] is still preferred over [110]. Note that at a given temperature, we have used a single set of parameters for each sample to fit the in-plane anisotropy and the FMR field, i.e., one set for //LSMO/LCO [lines in Fig. 3(a)] and one set for //LCO/LSMO [lines in Fig. 3(b)]. It is well known that STO distorts LSMO in such a way that in ultrathin LSMO, the easy direction turns along [100].[39] The present results show that LCO has a similar but a stronger effect on LSMO thin films. Similar values of the in-plane anisotropy constants are obtained for both kinds of bilayers. The isotropic behavior found by $M(H)$ loops in //LCO/LSMO bilayers may result from the tendency of manganite magnetization to point out of the plane in this sample. A large difference in K_{2c} depending on whether LCO is above or below LSMO is consistently found with FMR and magnetization loop data. They show that without shape anisotropy, the spins would favor perpendicular orientation when LSMO is grown on top of LCO. Also, the FMR was much broader (even beyond observation at certain B field directions) in this sample than in the other one, which is even consistent with small islands of perpendicular orientation (i.e., inhomogeneities with K_{2c} even defeating the shape anisotropy at some places).[38] The slow saturation of the H//plane magnetization curves in the //LCO/LSMO bilayer is consistent with this.

The magnetic behavior of single LSMO layers is usually discussed in the frame of structural distortions imposed by the substrate. It is known that bulk LSMO single crystals have [111] easy axes imposed by the rhombohedral distortion of its orthorhombic lattice, as reported by spin polarized electron microscopy of platelet-like samples.[37] Since the distortion occurs along the four diagonals of the cubic structure (there are four distortion axes along ⟨111⟩ directions), twinning of the crystals may result in four magnetic easy axes. Thin LSMO films on STO experience a tetragonal distortion in the plane that enlarges the in-plane parameters of LSMO to match the square in-plane lattice of STO. LSMO layers grown with cubic tensile epitaxial mismatch strain have a biaxial in-plane anisotropy with [110] easy axes and [100] hard axes.[30,33] It has been proposed that magnetic easy axes become the [110] directions, for they are the in-plane projections of the bulk ⟨111⟩ easy axes, made equivalent due to the tetragonal strain. Both //LCO/LSMO and //LSMO/LCO bilayers are epitaxial and uniformly strained. The reciprocal space maps do not evidence strain relaxation. On the other hand, a pure interfacial mechanism ruled by the magnetic interaction between manganite and cobaltite cannot be responsible for the change observed in magnetic anisotropy since this mechanism would be present for both bilayers. Thus we argue that the change in the out-of-plane lattice parameter may indicate a change in the structural (oxygen octahedra) distortions triggered by the different rotation pattern of the cobaltite. In this connection, the expanded lattice at the oxygen vacancy sites of the cobaltite (giving rise to the local undulations of the lattice planes discussed above and possibly also to the non-specular tails observed in the rocking curves) may trigger additional modifications of the pattern of structural distortions, which in turn produces modifications of the magnetic state. The effect on magnetic anisotropy results from changes in bandwidth and possibly orbital polarization, which have been shown to have a direct effect on magnetic anisotropy through the modified hopping rate, as discussed previously[5] to address the changes in magnetic anisotropy in LSMO grown on buffered $NdGaO_3$.

In summary, we have found that an ultrathin cobaltite buffer layer produces profound modifications in the magnetic anisotropy of LSMO layers. We propose that these changes are triggered by the structural effects of the cobaltite layer with a modified pattern of octahedral rotations which cause modifications in the magnetic interactions at the interface. An FMR experiment reveals an enhancement of the out-of-plane anisotropy term which indicates that magnetic interactions occurring at the interface with the cobaltite may trigger out-of-plane moments in the manganite. An exciting possibility is that they result from Dzyaloshinskii-Moriya interactions triggered by the strong spin orbit interaction of the cobaltite and the symmetry breaking associated with both the presence of the interface and distorted Mn–O–Mn bonds induced by octahedral rotations. Further studies will be conducted in future to clarify the effect of octahedral rotations on magnetic anisotropy at manganite cobaltite interfaces.

Work at UCM supported by Spanish MINECO through Grant Nos. MAT2014-52405-C02-01 and MAT2014-52405-C02-02 and by CAM through Grant No. CAM S2013/MIT-2740. M.V. and M.C. acknowledge support from Fundación BBVA and from MINECO through Grant

No. MAT2015-066888-C3-3-R. J.S. thanks the University Paris-Saclay (D'Alembert program) and CNRS for financing his stay at CNRS/Thales. T.F. acknowledges support from the Hungarian Research Fund OTKA No. K107228.

[1] J. Mannhart and D. G. Schlom, Science **327**, 1607 (2010).
[2] H. Y. Hwang, Y. Iwasa, M. Kawasaki, B. Keimer, N. Nagaosa, and Y. Tokura, Nat. Mater. **11**, 103 (2012).
[3] Y. Tokura and N. Nagaosa, Science **288**, 462 (2000).
[4] A. Bhattacharya and S. J. May, Annu. Rev. Mater. Res. **44**, 65 (2014).
[5] Z. Liao, M. Huijben, Z. Zhong, N. Gauquelin, S. Macke, R. J. Green, S. Van Aert, J. Verbeek, G. Van Tendeloo, K. Held, G. A. Sawatzky, G. Koster, and G. Rijnders, Nat. Mater. **15**, 425 (2016).
[6] D. Kan, R. Aso, R. Sato, M. Haruta, H. Kurata, and Y. Shimakawa, Nat. Mater. **15**, 432 (2016).
[7] R. Gao, Y. Dong, H. Xu, H. Zhou, Y. Yuan, V. Gopalan, C. Gao, D. D. Fong, Z. Chen, Z. Luo, and L. W. Martin, ACS Appl. Mater. Interfaces **8**, 14871 (2016).
[8] A. M. Glazer, Acta Crystallogr., Sect. B: Struct. Crystallogr. Cryst. Chem. **28**, 3384 (1972).
[9] A. M. Glazer, Acta Crystallogr., Sect. A: Found. Adv. **31**, 756 (1974).
[10] B. Rivas-Murias, I. Lucas, P. Jimenez-Cavero, C. Magen, L. Morellon, and F. Rivadulla, Nano Lett. **16**, 1736 (2016).
[11] Z. Sefrioui, C. Visani, M. J. Calderón, K. March, C. Carretero, M. Walls, A. Rivera-Calzada, C. Leon, R. Lopez-Anton, T. R. Charlton, F. A. Cuellar, E. Iborra, F. Ott, D. Imhoff, L. Brey, M. Bibes, J. Santamaria, and A. Barthelemy, Adv. Mater. **22**, 5029 (2010).
[12] G. Sanchez-Santolino, J. Tornos, D. Hernandez-Martin, J. I. Beltran, C. Munuera, M. Cabero, A. Perez-Muñoz, J. Ricote, F. Mompean, M. Garcia-Hernandez, Z. Sefrioui, C. Leon, S. J. Pennycook, M. C. Muñoz, M. Varela, and J. Santamaria, Nat. Nanotechnol. **12**, 655 (2017).
[13] D. Khomskii, *Transition Metal Compounds* (Cambridge University Press, 2014).
[14] P. M. Raccah and J. B. Goodenough, Phys. Rev. **155**, 932 (1967).
[15] V. G. Bhide, D. S. Rajoria, G. R. Rao, and C. N. R. Rao, Phys. Rev. B **6**, 1021 (1972).
[16] M. A. Korotin, S. Yu. Ezhov, I. V. Solovyev, V. I. Anisimov, D. I. Khomskii, and G. A. Sawatzky, Phys. Rev. B **54**, 5309 (1996).
[17] S. Noguchi, S. Kawamata, K. Okuda, H. Nojiri, and M. Motokawa, Phys. Rev. B **66**, 094404 (2002).
[18] A. Podlesnyak, S. Streule, J. Mesot, M. Medarde, E. Pomjakushina, K. Conder, A. Tanaka, M. W. Haverkort, and D. I. Khomskii, Phys. Rev. Lett. **97**, 247208 (2006).
[19] M. W. Haverkort *et al.*, Phys. Rev. Lett. **97**, 176405 (2006).
[20] D. Fuchs, C. Pinta, T. Schwarz, P. Schweiss, P. Nagel, S. Schuppler, R. Schneider, M. Merz, G. Roth, and H. V. Löhneysen, Phys. Rev. B **75**, 144402 (2007).
[21] J. W. Freeland, J. X. Ma, and J. Shi, Appl. Phys. Lett. **93**, 212501 (2008).
[22] V. V. Mehta, M. Liberati, F. J. Wong, R. V. Chopdekar, E. Arenholz, and Y. Suzuki, J. Appl. Phys. **105**, 07E503 (2009).
[23] H. Hsu, P. Blaha, and R. M. Wentzcovitch, Phys. Rev. B **85**, 140404(R) (2012).
[24] J. M. Rondinelli and N. A. Spaldin, Phys. Rev. B **79**, 054409 (2009).
[25] W. S. Choi, J.-H. Kwon, H. Jeen, J. E. Hamann-Borrero, A. Radi, S. Macke, R. Sutarto, F. He, G. A. Sawatzky, V. Hinkov, M. Kim, and H. N. Lee, Nano Lett. **12**, 4966 (2012).
[26] N. Biskup, J. Salafranca, V. Mehta, M. P. Oxley, Y. Suzuki, S. J. Pennycook, S. T. Pantelides, and M. Varela, Phys. Rev. Lett. **112**, 087202 (2014).
[27] V. V. Mehta, N. Biskup, C. Jenkins, E. Arenholz, M. Varela, and Y. Suzuki, Phys. Rev. B **91**, 144418 (2015).
[28] J. Fujioka, Y. Yamasaki, H. Nakao, Y. Murakami, M. Nakamura, M. Kawasaki, and Y. Tokura, Phys. Rev. Lett. **111**, 027206 (2013).
[29] F. Y. Bruno, J. Garcia-Barriocanal, M. Varela, N. M. Nemes, P. Thakur, J. C. Cezar, N. B. Brookes, A. Rivera-Calzada, M. Garcia-Hernandez, C. Leon, S. Okamoto, S. J. Pennycook, and J. Santamaria, Phys. Rev. Lett. **106**, 147205 (2011).
[30] G. Sanchez-Santolino, M. Cabero, M. Varela, J. Garcia-Barriocanal, C. Leon, S. J. Pennycook, and J. Santamaria, Microsc. Microanal. **20**, 825 (2014).
[31] J. Gazquez, S. Bose, M. Sharma, M. A. Torija, S. J. Pennycook, C. Leighton, and M. Varela, APL Mater. **1**, 012105 (2013).
[32] Y. Suzuki, H. Y. Hwang, S.-W. Cheong, and R. B. van Dover, Appl. Phys. Lett. **71**, 140 (1997).
[33] Y. Suzuki, H. Y. Hwang, S.-W. Cheong, T. Siegrist, R. B. van Dover, A. Asamitsu, and Y. Tokura, J. Appl. Phys. **83**, 7064 (1998).
[34] M. Mathews, F. M. Postma, J. C. Lodder, R. Jansen, G. Rijnders, and D. H. A. Blank, Appl. Phys. Lett. **87**, 242507 (2005).
[35] K. Steenbeck and R. Hiergeist, Appl. Phys. Lett. **75**, 1778 (1999).
[36] E. P. Houwman, G. Maris, G. M. De Luca, N. Niermann, G. Rijnders, D. H. A. Blank, and S. Speller, Phys. Rev. B **77**, 184412 (2008).
[37] M. Konoto, T. Kohashi, K. Koike, T. Arima, Y. Kaneko, Y. Tomioka, and Y. Tokura, Appl. Phys. Lett. **84**, 2361 (2004).
[38] A. Alberca, N. M. Nemes, F. J. Mompean, T. Fehér, F. Simon, J. Tornos, C. Leon, C. Munuera, B. J. Kirby, M. R. Fitzsimmons, A. Hernando, J. Santamaria, and M. Garcia-Hernandez, Phys. Rev. B **88**, 134410 (2013).
[39] N. M. Nemes, M. Garcia-Hernandez, Z. Szatmári, T. Fehér, F. Simon, C. Visani, V. Peña, C. Miller, J. Garcia-Barriocanal, F. Bruno, Z. Sefrioui, C. León, and J. Santamaria, IEEE Trans. Magn. **44**(11), 2926 (2008).